Structures of small Ti- and V-doped Pt clusters : A GA-DFT study

Jennings, Paul; Johnston, R.L.

DOI:
10.1016/j.comptc.2013.06.033

Computational and Theoretical Chemistry 1021 (2013) 91–100

Contents lists available at SciVerse ScienceDirect

Computational and Theoretical Chemistry

journal homepage: www.elsevier.com/locate/comptc

Structures of small Ti- and V-doped Pt clusters: A GA-DFT study ☆

P.C. Jennings [a], R.L. Johnston [b,*]

[a] School of Chemical Engineering, University of Birmingham, Edgbaston, Birmingham B15 2TT, UK
[b] School of Chemistry, University of Birmingham, Edgbaston, Birmingham B15 2TT, UK

ARTICLE INFO

Article history:
Received 17 May 2013
Received in revised form 25 June 2013
Accepted 25 June 2013
Available online 5 July 2013

Keywords:
Clusters
Platinum
Titanium
Vanadium
GA-DFT

ABSTRACT

High level GA-DFT searches are performed on small platinum clusters doped with early transition metal atoms, $Pt_{x-y}M_y$ (M = Ti, V), where $x = 2–6$, $y = 1, 2$. Spin effects are studied and the global minimum structures are presented for the various spin multiplicities. It is found that varying spin can have significant effects on the pure Pt clusters, while spin has less effect for the doped clusters.

1. Introduction

Nano- and sub-nanoscale clusters are of scientific interest due to distinct optical, magnetic, and catalytic properties which differ from bulk materials [1]. The application of nanoclusters in catalysis is a growing field of research [2]. An area of particular recent interest is catalysis on bi- and multi-metallic nanoparticles (“nanoalloys”) [1,3,4] – where catalytic properties can be tuned by varying the size, shape, elemental composition and chemical ordering of the nanoparticles.

Platinum (Pt) based nanoclusters are amongst the most interesting and have been widely investigated due to their wide ranging use in heterogeneous catalysis. The utilisation of Pt for numerous reactions e.g. oxygen reduction reaction (ORR) and hydrogen oxidation reaction (HOR) in the Proton Electrolyte Fuel Cell (PEFC), has driven the investigation of small to large Pt nanoclusters as well as extensive work on bulk Pt [5–7].

Due to the high cost of Pt and other platinum group metals the study of heterogeneous nanoalloy systems has become increasingly important. As well as intrinsic cost reductions through preparation of heterogeneous systems, especially when alloying with nonprecious metals, it is also possible to improve catalytic reactivity and durability. We have previously reported the analysis of Pt and titanium (Ti) nanoalloys with the eventual aim of reducing PEFC electrocatalyst costs as well as improving reactivity [8,9]. Promise has also been shown by Pt nanoalloys with other early transition metals, including vanadium (V) [6,10–13].

Previous studies have revealed a number of different growth patterns of small Pt clusters, as well as disagreement over the size at which the lowest energy structure changes from 2D to 3D [14–17]. For example, whilst Sebetci found 3D cluster geometries to be favourable as low as Pt_4 using the Becke, three-parameter, Lee–Yang–Parr (B3LYP) exchange–correlation (xc) functional [18], Bhattacharyya and Majumder predicted the 2D-3D transition to occur between Pt_9 and Pt_{10} using the projected augmented wave (PAW) method [19].

Whilst some theoretical studies have been reported on pure Ti clusters [20,21], to our knowledge, little has been performed on Pt clusters doped with early transition metals. Here, we use a novel Genetic Algorithm (GA) coupled with Density Functional Theory (DFT) approach to search for Pt clusters with 2–6 atoms. We then investigate the effects of doping with the early transition metals Ti and V.

2. Methodology

Simulations of nanoclusters present complex issues, especially when modelling transition metals. Several techniques have been employed to quickly and accurately compute the physical and chemical properties of nanoclusters with a range of compositions and sizes. The technique used is generally determined by a combination of the desired property and the size and composition

* Corresponding author. Tel.: +44 0 121 414 7477; fax: +44 0 121 414 4403.
E-mail addresses: p.c.jennings@pgr.bham.ac.uk (P.C. Jennings), r.l.johnston@bham.ac.uk (R.L. Johnston).
URL: http://www.tc.bham.ac.uk/~roy/ (R.L. Johnston).

2210-271X/$ - see front matter © 2013 The Authors. Published by Elsevier B.V. All rights reserved.
http://dx.doi.org/10.1016/j.comptc.2013.06.033

Table 1
Relative energies (E_{rel}) and bond lengths for the pure dimers M_2, for varying spin multiplicities (2S + 1).

M	2S + 1	E_{rel} (eV)	M–M (Å)
Ti	1	0.00	1.93
	3	−0.23	1.90
	5	−0.05	1.97
	7	0.13	2.39
	9	0.50	2.37
V	1	0.00	1.74
	3	−0.23	1.74
	5	0.25	1.73
	7	0.89	1.89
	9	0.64	2.52
Pt	1	0.00	2.34
	3	−0.30	2.34
	5	0.17	2.32
	7	2.58	2.36
	9	5.18	2.34

Table 2
Relative energies (E_{rel}) and bond lengths for the heteronuclear Pt–M dimers at varying spin multipleicities (2S + 1).

M	2S + 1	E_{rel} (eV)	Pt–M (Å)
Ti	1	0.00	2.12
	3	−0.47	2.13
	5	0.48	2.40
	7	1.81	2.68
	9	4.14	2.90
V	2	0.00	2.14
	4	−0.35	2.18
	6	0.37	2.39
	8	1.55	2.66
	10	3.76	2.83

of the cluster. For example, search algorithms can be used to find low energy structures for pure and alloyed systems of between a few and several hundred atoms. Common search techniques include basin-hopping algorithms, stochastic-search methods and genetic algorithms coupled with an empirical potential e.g. Gupta, Sutton-Chen and Murrell-Mottram [22–24].

GAs are search methods for function minimisation, which are based on principles akin to natural evolution. The algorithm utilises operators analogous to those observed in nature (mating, mutation and natural selection) to explore the multidimensional potential energy surface (PES) [25]. Empirical potentials, such as those mentioned above, can be used to search for low energy structures on the PES although they tend to favour 3D structures with high symmetry. This may be relatively accurate for clusters with sizes of more than 20 atoms, however certain smaller clusters tend to favour 2D structures [26], making the use of empirical potentials for small systems questionable.

Ab initio simulations, which are able to explicitly treat electrons, have been used to successfully compute structural properties of transition metal clusters. DFT calculations have been acknowledged as one of the best methods for performing relatively accurate simulations on metallic clusters [27]. DFT can generally describe the PES more accurately than empirical potentials and so is able to predict the likely low energy structures of small nanoclusters. In this work, a GA-DFT approach is employed to accurately search for energetically low lying structures.

The GA-DFT approach, which has been described elsewhere [26,28,29], uses the Birmingham Cluster Genetic Algorithm (BCGA) [30,25] coupled with the PWscf plane wave DFT code in the quantum chemistry package Quantum-Espresso [31]. An initial generation is produced by randomly placing atoms in a sphere. The atoms are then transferred to a centre of mass coordinate system and placed in the centre of the unit cell. The cluster is locally relaxed until convergence is achieved: if the convergence criteria are not

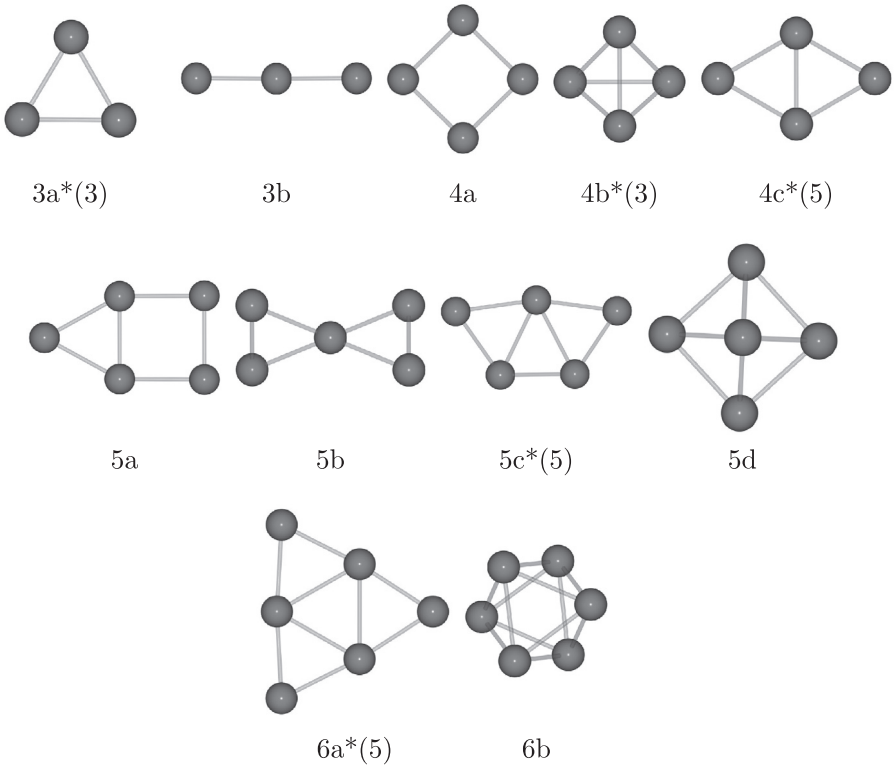

Fig. 1. Low energy structures found for pure Pt clusters, from Pt_3 to Pt_6, with varying spin. GM clusters for all sizes are specified (*). Numbers in brackets show at which spin multiplicity the GM is found.

Table 3
Relative energies (E_{rel}) and average bond distances for the low energy Pt_3 to Pt_6 clusters (shown in Fig. 1), with varying spin multiplicities (2S + 1).

2S + 1	Cluster	E_{rel} (eV)	Pt–Pt (Å)
Pt_3			
1	3a	0.00	2.47
3	3a	−0.09	2.50
5	3b	0.51	2.37
7	3a	1.69	2.51
9	3a	6.04	2.50
Pt_4			
1	4a	0.00	2.46
1	4c	0.01	2.52
3	4b	−0.32	2.60
3	4c	−0.29	2.53
5	4c	−0.32	2.52
7	4a	−0.04	2.45
9	4b	1.88	2.61
Pt_5			
1	5a	0.00	2.48
1	5b	0.00	2.47
3	5c	−0.15	2.53
5	5c	−0.29	2.54
7	5d	−0.15	2.58
9	5d	0.66	2.62
Pt_6			
1	6a	0.00	2.53
3	6a	−0.15	2.53
5	6a	−0.19	2.54
7	6a	−0.03	2.54
9	6b	0.47	2.64

Table 4
Relative energies (E_{rel}), average bond lengths and average Bader charges for singly doped PtTi clusers (shown in Fig. 2), for varying spin multiplicities (2S + 1).

2S + 1	Cluster	E_{rel} (eV)	Pt–Pt (Å)	Pt–Ti (Å)	Ave. Pt Charge |e|	Ave. Ti Charge |e|
Pt_2Ti						
1	3a	0.00	–	2.14	−0.68	1.41
3	3b	0.96	2.83	2.21	−0.52	1.10
5	3b	2.42	2.59	2.38	−0.46	0.58
7	3b	4.09	2.40	2.62	−0.32	0.70
9	3c	7.58	2.31	3.10	−0.06	0.10
Pt_3Ti						
1	4a	0.00	2.70	2.26	−0.44	1.28
1	4b	0.03	2.56	2.27	−0.45	1.45
3	4a	0.43	2.77	2.25	−0.45	1.37
5	4a	1.67	2.57	2.41	−0.39	1.23
7	4c	3.18	2.48	2.43	−0.29	0.98
7	4a	3.19	2.47	2.62	−0.30	1.01
9	4a	5.06	2.56	2.70	−0.24	0.83
Pt_4Ti						
1	5a	0.00	2.63	2.35	−0.36	1.51
3	5a	0.05	2.60	2.35	−0.35	1.46
5	5b	0.89	2.62	2.43	−0.32	1.36
5	5c	0.89	2.68	2.38	−0.32	1.28
7	5b	2.06	2.65	2.49	−0.31	1.24
9	5b	3.72	2.60	2.65	−0.24	1.07
9	5d	3.75	2.64	2.57	−0.24	1.13
Pt_5Ti						
1	6a	0.00	2.62	2.42	−0.29	1.60
1	6b	0.05	2.65	2.41	−0.29	1.44
3	6a	−0.15	2.61	2.42	−0.29	1.43
5	6b	0.34	2.62	2.43	−0.29	1.43
7	6b	1.62	2.65	2.47	−0.27	1.42
7	6c	1.65	2.60	2.43	−0.28	1.54
9	6d	2.67	2.63	2.53	−0.23	1.20
9	6e	2.68	2.58	2.45	−0.24	1.19

met a new random structure is generated. After all members of the generation have been minimised, the energetically lowest members are selected and taken forward. These energetically favourable members of the population are mated and mutated to form novel structures for the next generation. This process is repeated until the energy of the lowest lying isomer is considered to have converged.

Using the GA-DFT method, it is possible to accurately search the PES of the system being studied. Following the structural search, re-minimisations are performed on all unique structures, using the quantum chemistry code NWChem [32]. As well as re-minimising, other properties have also been studied using NWChem, e.g. spin effects, investigating multiplicities up to the nonet. Since there is no guarantee that the structures generated using this approach are actually local minima rather than transition states or higher rank saddle points, following the structural search, a frequency analysis is performed. Frequency analysis was performed using NWChem after re-minimisation for varying multiplicities.

For the lowest lying isomers, Bader charge analysis is performed. Bader charge analysis is utilised to elucidate general trends in charge transfer. This quantitatively suggests the direction of charge transfer, although values are not suggested to be physically accurate.

3. Computational details

The GA was run with a population size of 10 clusters and termination upon convergence was set at five generations. This means that if the energy of the lowest energy cluster per generation was within 0.01 eV for five generations, convergence was said to have been achieved.

All GA-DFT simulations were performed using the PWscf plane wave DFT code in the quantum chemistry package Quantum-Espresso 4.3.2. The PWscf calculations were performed using ultrasoft Perdew–Burke–Ernzerhof (PBE) xc functional, accounting for 12 ($3s^2$, $3p^6$, $3d^2$, $4s^2$), 13 ($3s^2$, $3p^6$, $3d^3$, $4s^2$) and 10 ($5d^9$, $6s^1$) valence electrons for Ti, V and Pt, respectively. Scalar relativistic corrections are employed for all pseudopotentials, while the Pt potential also contains non-linear core correction and Ti and V potentials contain semi-core states.

A kinetic energy (E_k) cutoff for the wavefunctions of 55.0 Ry was used, and the supercell dimensions were taken to be sufficiently large to remove the possibility of interactions with neighbouring clusters, however not so large as to be detrimental to calculation speed. When performing structural searches, E_k cutoff for the charge density was set at 500.0 Ry. The convergence threshold for self consistency was also set at 10^{-5} Ry, whilst Marzari–Vanderbilt Gaussian smearing was set at 0.002 Ry.

Following the initial structural searches, further structural relaxation and frequency analysis was performed using the DFT code in the quantum chemistry package NWChem 6.1. This analysis was performed using the PBE xc functional and spherical Gaussian type-orbital triple-zeta (TZVP) basis sets. All electron calculations were performed on Ti and V atoms while an effective core potential (accounting for 60 electrons) was employed for Pt.

4. Results and discussion

4.1. Dimers

A number of dimers were studied, including pure M_2 (M = Ti, V, Pt) and alloyed Pt-M (M = Ti, V), the results of which can be seen in Tables 1 and 2 for the pure and alloyed dimers, respectively. In all cases, the energies are given relative to the lowest energy structures found for the lowest spin state (singlet or doublet). When analysing the results for the pure dimers, several trends become apparent. Firstly, for the Ti, V and Pt dimers, triplet states are found

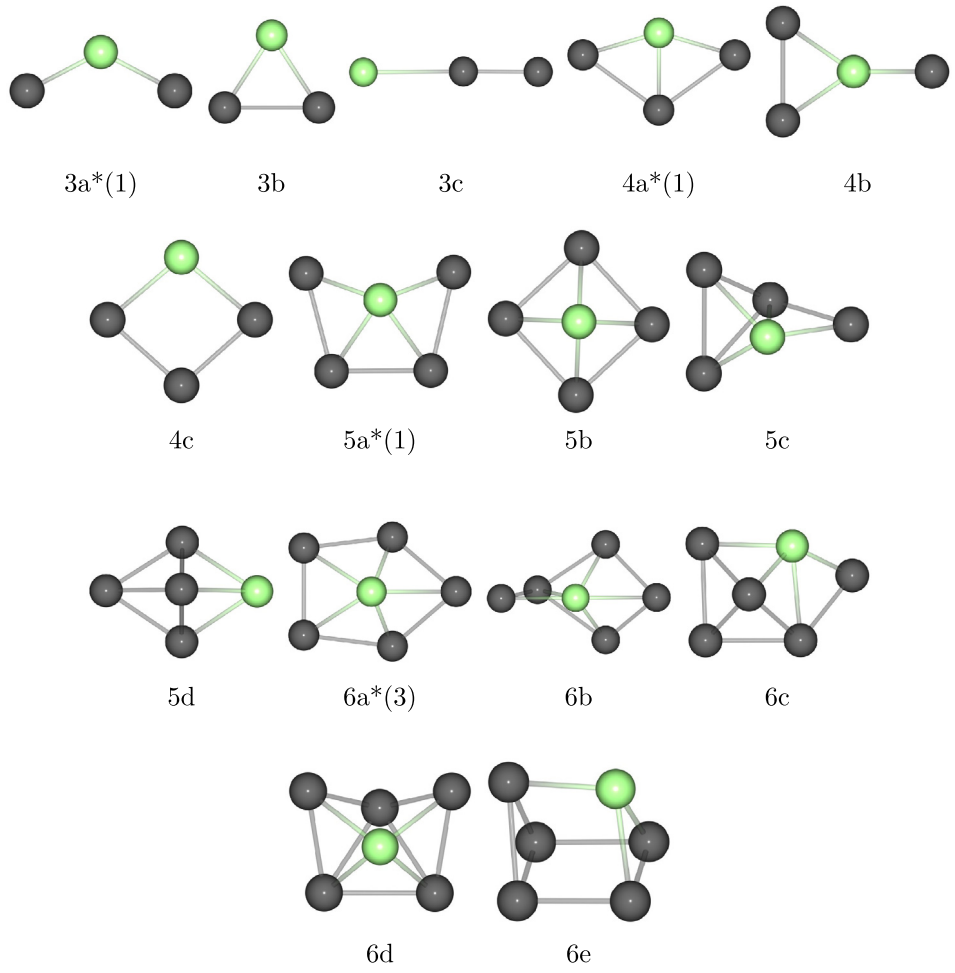

Fig. 2. Low energy structures found for $Pt_{x-1}Ti$ clusters, from Pt_2Ti_1 to Pt_5Ti_1, with varying spin multiplicities. GM clusters for all sizes are specified (*). Numbers in brackets show at which spin multiplicity the GM is found.

to be energetically favourable, with higher multiplicities generally being less favourable than the singlet.

When comparing bond lengths, increasing the spin multiplicity, generally results in bond elongation for the Ti and V dimers. The bond lengths for Pt_2 remain relatively constant, even for the high spin multiplicities, although the energetic penalty paid to access these higher spin states is greater than for Ti_2 and V_2.

For the Pt-M dimers, a triplet or quartet is found to be energetically favourable for PtTi and PtV, respectively, with higher miltiplicities being less favourable than a singlet or doublet. All Pt-M bond lengths are found to be greater than in the corresponding M_2 dimers, though smaller than the Pt_2 dimer. Once again, as the multiplicity is increased, the bond length also increases.

Results for Pt_2 are in good agreement with experimental and theoretical work. Experimental studies have determined a Pt–Pt bond length of 2.33 Å [33], close to the 2.34 Å calculated for the lowest energy Pt dimer. This is also in good agreement with other DFT studies, which have predicted the triplet state to be the lowest in energy [34]. It has been found that DFT calculations tend to underestimate the Ti_2 and V_2 bond lengths [35]. Our calculated dimer bond lengths are 1.90 and 1.74 Å for Ti_2 and V_2, respectively, compared with experimental values of 1.94 and 1.78 Å [36,37].

4.2. Pt clusters

The energetically favourable structures for the pure Pt clusters can be seen in Fig. 1, with their relative energies displayed in Table 3: energetically competitive structures are also displayed for a more complete discussion. In previous discussions of small Pt clusters, it has been noted that results do not always converge on the same structures, with different studies finding different global minimum (GM) clusters. It has been suggested that this is due to the use of different pseudopotentials, basis sets XC functionals and energy cutoffs [14].

GM clusters are discussed with respect to the minimum energy cluster for a given size. It was expected that the 3-atom clusters, would preferentially form triangular D_{3h} structures (*3a*). For all spin multiplicities other than 5 this was found to be the case. However, for a spin multiplicity of 5, the linear conformation (*3b*) was 0.2 eV lower in energy than the triangular structure. The GM is still found for the triangular D_{3h} structure at the triplet state, with a Pt–Pt–Pt angle of 60.0°. Although there is little difference between the singlet and triplet energies.

For Pt_4 clusters there is competition between the triplet T_d tetrahedron (*4b*) and the quintet C_{2v} butterfly (*4c*), though this structure is only 30 meV higher in energy than the tetrahedron in the triplet state. For Pt_5, the GM is found to be the C_2 W-shaped cluster (*5c*) in the quintet state. This is found to be at least 0.14 eV more stable than other isomers. Finally, the quintet triangular D_{3h} structure (*6a*) is found to be the GM for Pt_6.

Whilst for Pt_3, there is little advantage in increasing the spin multiplicity, for the larger clusters, higher spin states (up to septet) are favoured. For the nonet states, relatively large energetic penalties are observed for all the pure Pt clusters, though this penalty decreases with increased cluster size.

Table 5
Relative energies (E_{rel}), average bond lengths and average Bader charges for doubly doped PtTi clusters (shown in Fig. 3), for varying multiplicities (2S + 1).

2S + 1	Cluster	E_{rel} (eV)	Pt–Pt (Å)	Pt–Ti (Å)	Ti–Ti (Å)	Ave. Pt Charge |e|	Ave. Ti Charge |e|
$PtTi_2$							
1	3a	0.00	–	2.42	2.09	−0.85	0.52
3	3a	−0.08	–	2.43	2.12	−0.85	0.41
5	3a	0.09	–	2.45	2.03	−0.88	0.47
7	3a	0.44	–	2.18	2.28	−0.95	0.56
9	3a	2.63	–	2.45	2.38	−0.68	0.38
Pt_2Ti_2							
1	4a	0.00	–	2.42	2.19	−0.89	0.85
3	4a	0.04	–	2.43	2.26	−0.91	1.00
5	4a	0.23	–	2.41	2.53	−0.89	0.87
7	4b	1.89	2.71	2.45	2.54	−0.73	0.69
9	4b	3.60	2.51	2.59	2.46	−0.60	0.66
Pt_3Ti_2							
1	5a	0.00	–	2.41	2.30	−0.79	1.27
3	5a	0.68	–	2.39	2.55	−0.79	1.23
5	5b	1.63	2.67	2.43	2.65	−0.76	1.08
7	5c	2.80	2.70	2.48	2.73	−0.68	1.01
9	5d	4.56	2.63	2.49	2.36	−0.46	0.76
Pt_4Ti_2							
1	6a	0.00	–	2.37	2.74	−0.86	1.25
3	6b	0.51	2.62	2.35	2.65	−0.63	1.41
5	6c	1.24	2.60	2.48	2.60	−0.61	1.30
7	6d	2.34	2.60	2.51	2.65	−0.60	1.28
9	6e	3.95	2.65	2.54	2.41	−0.42	0.91

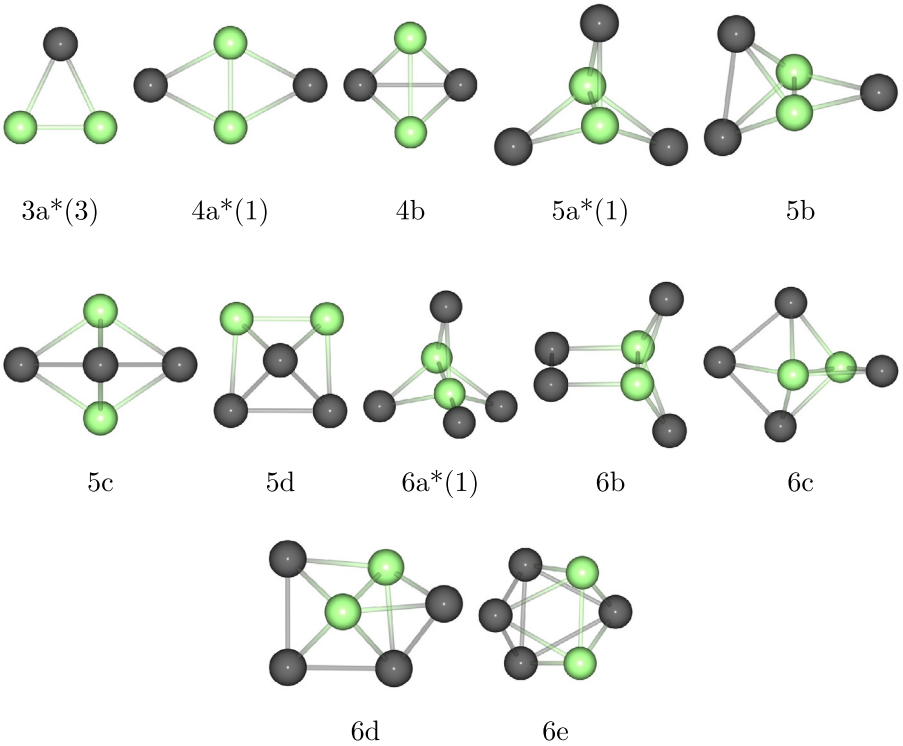

Fig. 3. Low energy structures found for $Pt_{x-2}Ti_2$ clusters, from $PtTi_2$ to Pt_4Ti_2, with varying spin multiplicities. GM clusters for all sizes are specified (*). Numbers in brackets show at which spin multiplicity the GM is found.

From the results obtained in this study, no clear 2D/3D transition can be identified. Whilst the 3 and 6 atom GM are predicted to be planar (D3h) triangles, other structures identified as GM tend to have more deformed (twisted, or puckered) structures. For the Pt_2 dimer, there was little change in the Pt-Pt bond length with changing spin, this trend is continued for Pt_3 and Pt_4. However, for the larger cluster sizes, the average bond length increases with increasing spin.

As mentioned previously, small differences in the computational methodology can result in differences in the predicted GM structures. The methodology employed in this work differs from others [14–19], with the use of a LCAO based DFT code, TZVPD

Table 6
Relative energies (E_{rel}), average bond lengths and average Bader charges for the singly doped PtV clusters (shown in Fig. 4), with varying spin multiplicities (2S + 1).

2S + 1	Cluster	E_{rel} (eV)	Pt–Pt (Å)	Pt–V (Å)	Ave. Pt Charge |e|	Ave. V Charge |e|
Pt_2V						
2	3a	0.00	–	2.13	−0.60	0.69
4	3a	0.94	–	2.21	−0.48	1.01
6	3b	1.58	2.55	2.39	−0.41	0.79
8	3b	2.87	2.41	2.60	−0.27	0.37
10	3a	5.46	–	2.66	−0.12	0.36
Pt_3V						
2	4a	0.00	2.89	2.16	−0.41	1.12
2	4b	0.07	2.70	2.25	−0.37	1.12
4	4b	0.40	2.58	2.33	−0.35	1.09
6	4b	1.15	2.52	2.45	−0.32	0.82
6	4c	1.17	2.71	2.35	−0.36	1.16
8	4c	2.12	2.63	2.50	−0.29	0.82
8	4d	2.12	2.48	2.42	−0.28	0.90
10	4c	3.75	2.56	2.70	−0.19	0.61
10	4d	3.75	2.43	2.60	−0.19	0.71
Pt_4V						
2	5a	0.00	2.59	2.27	−0.33	1.43
2	5b	0.06	2.71	2.25	−0.31	1.27
4	5b	0.25	2.59	2.34	−0.31	1.32
6	5b	1.05	2.53	2.44	−0.26	1.08
8	5b	2.05	2.49	2.56	−0.25	1.16
8	5c	2.05	2.58	2.44	−0.27	1.07
10	5d	2.84	2.60	2.54	−0.21	0.87
Pt_5V						
2	6a	0.00	2.67	2.32	−0.27	0.96
4	6b	0.31	2.57	2.35	−0.25	1.38
6	6a	0.91	2.56	2.47	−0.23	1.00
6	6c	0.92	2.62	2.41	−0.26	1.34
6	6b	0.93	2.53	2.45	−0.23	1.23
8	6d	1.46	2.58	2.36	−0.20	1.20
8	6e	1.46	2.61	2.49	−0.22	0.93
10	6d	2.17	2.56	2.49	−0.18	1.09

basis set and PBE XC for the final energetic analysis. All structures noted in previous studies were located in the GA-DFT search, although in some cases different energetic ordering was found.

4.3. Pt–Ti clusters

4.3.1. Singly doped

The lowest lying structures for the singly doped PtTi clusters are listed in Table 4, corresponding to the structures in Fig. 2. For Pt_2Ti, the open bent C_{2v} structure (*3a*) is favourable for the singlet state, with a Pt–Ti–Pt angle of 124.6°. The bonding angle is reduced in the triplet state, to 79.6°, producing the closed C_{2v} triangle structure (*3b*) with a Pt–Pt bond, 0.96 eV higher in energy than the singlet. The closed triangle remains the lowest energy structure for the quintet and septet states. The cluster then opens up again (*3c*) for the nonet state, producing a more linear cluster.

Different energetic trends are observed for the Pt_3 and Pt_2Ti clusters. The GM is a triplet state for Pt_3 and a singlet state when doped with a single Ti atom. Energetic penalties are observed for higher spin multiplicities compared to the singlet state. These penalties are found to be larger for Pt_2Ti than Pt_3.

For Pt_3Ti, the GM is a singlet, with the C_{2v} kite (*4a*) and C_s Y-shape (*4b*) isomers being energetically competitive. Significant energetic penalties are associated with increasing spin multiplicity, in contrast to Pt_2Ti and Pt_4. For Pt_4, the triplet and quintet states produce competitive GM structures, with even the septet state being 40 meV more favourable than the singlet. Once doped with a single Ti atom, this behaviour changes, making the higher spin multiplies unfavourable. The septet state is 3.18 eV higher in energy than the singlet Pt_3Ti.

Once again, for Pt_4Ti the GM is found for the singlet state. A W-shape structure (*5a*) with no symmetry is found to be the GM, this is a similar structure to that of Pt_5. However, once again higher spin multiplies incur an energetic penalty compared to the singlet state, although not as much as for Pt_3Ti.

Unlike the three, four and five atom clusters, the triplet state is found to be most favourable for Pt_5Ti. This results in the triplet C_s twisted pentagonal structure (*6a*) being the most energetically favourable structure. For larger cluster sizes, the energetic penalties associated with higher spin states is reduced. For Pt_5Ti it is then found that the Ti doped clusters behave more like the pure Pt clusters, with higher spin states (triplet) becoming more favourable.

Due to charge transfer the lowest energy homotops tend to maximise the number of Pt–Ti bonds, with Ti atoms in the most highly-connected sites. As with the pure Pt clusters, the GM isomers identified for $Pt_{x-1}Ti$ are planar, or "bent-planar" structures for cluster sizes 3–6. As the multiplicity is increased, there is generally little change in the average Pt–Pt bond length, though there is a slight increase in the average Pt–Ti bond lengths.

When analysing the Bader charges, significant charge transfer is seen from the Ti, which becomes highly positive (as high as +1.60), to the Pt atoms, which become negative. As expected, on increasing the cluster size, the Pt generally becomes slightly less negatively charged, whilst the Ti generally becomes slightly more positively charged. There is a decrease in charge transfer as the spin multiplicity is increased. The average Pt charge is 0.25 less negative and Ti is an average 0.64 less positive.

4.3.2. Doubly doped

The lowest lying structures for doubly doped PtTi clusters are listed in Table 5, corresponding to the structures in Fig. 3. The closed C_{2v} triangle (*3a*) is found preferentially for all multiplicites for the $PtTi_2$ clusters. Unlike for Pt_2Ti, the GM is found for the triplet state, with a Ti–Pt–Ti angle of 51.7°. For $PtTi_2$ relatively small energy penalties are found for higher spin states.

This situation is different for the larger doubly doped clusters, with the GM being found for the singlet state in all cases. The observed bonding motifs suggest preferential formation of Ti–Ti bonds, followed by Pt–Ti bonding, and it appears that greater Pt–Pt bonding results in less favourable structures. For the C_{2v} butterfly Pt_2Ti_2 GM structure (*4a*), there are no Pt–Pt bonds. The C_{2v} tetrahedron structure (*4b*) with a single Pt–Pt bond is only found to be locally stable at higher spin multiplicities (5–9).

The singlet D_{3h} structure (*5a*) is found to be the GM for Pt_3Ti_2. The lowest energy homotop again favours Ti–Ti and Pt–Ti bonding, with Pt-Pt bonding found to be unfavourable, with the same being true for the singlet C_{3v} structure (*6a*), which is the GM for Pt_4Ti_2. With increasing cluster size, the energetic penalty associated with increasing the spin multiplicity initially increases, although it decreases again for Pt_4Ti_2. The lowest penalties (and the triplet state GM) are found for the three atom clusters, with the largest penalties associated with the five atom clusters. It is expected that as the cluster size increases, and Pt/Ti ratio increases, higher spin states (than the singlet) will again be lower in energy (as with Pt_5Ti), although this is not seen in the 3–6 atom range.

For the 3–5 atom clusters, growth occurs with additional Pt atoms bonding to a central Ti_2 unit. This minimises Pt–Pt interactions, whilst maximising Pt–Ti interactions. Following filling of the Ti–Ti bridge positions, it is seen that additional Pt atoms favour bonding to the Ti top sites, as in Pt_4Ti_2. Due to the lack of Pt–Pt bonding, it is difficult to draw conclusions from the average Pt–Pt bond lengths. However, in general, as the spin multiplicity is increased, the Pt–Ti bond length increases. The same appears

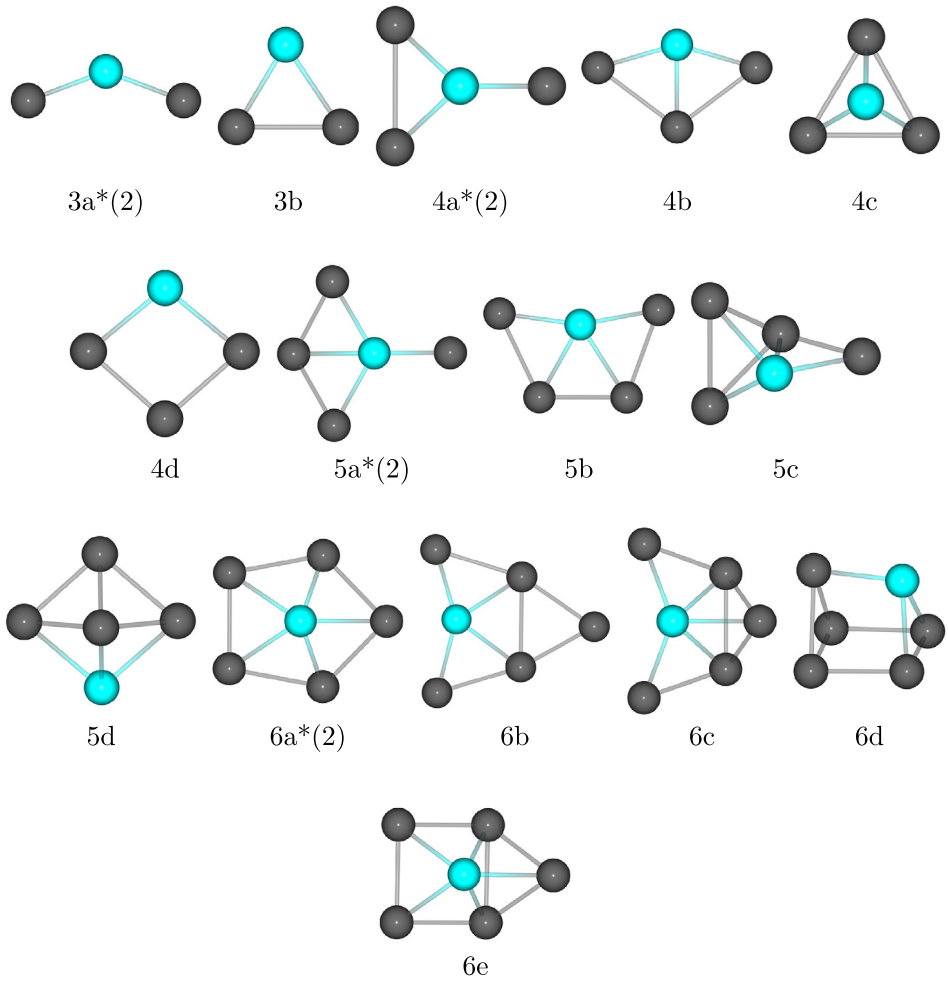

Fig. 4. Low energy structures found for singly doped $Pt_{x-1}V$ clusters, from Pt_2V_1 to Pt_5V_1, with varying spin multiplicities. GM clusters for all sizes are specified (*). Numbers in brackets show at which spin multiplicity the GM is found.

to be true for the average Ti–Ti bond length. For Pt_4Ti_2, as the spin is increased the average Ti–Ti bond length generally decreases. The doubly doped PtTi clusters, have a distinct 2D/3D transition between Pt_2Ti_2 and Pt_3Ti_2.

The Bader charge analysis demonstrates significant charge transfer from Ti to Pt. Once again, as the spin is increased, the charge transfer decreases, though there is less change in charge transfer with changing cluster size, compared to the singly doped PtTi clusters.

4.4. Platinum vanadium clusters

4.4.1. Singly doped

The lowest lying structures for the singly doped PtV clusters are given in Table 6, corresponding to the structures shown in Fig. 4. From the energetic analysis, it is found that in all cases, a spin multiplicity of 2 (the lowest possible) is favoured. This differs from the monometallic and alloyed dimers, where the triplet or quartet states were found to be most stable. Furthermore, as the cluster size increases, the energetic penalty associated with higher spin states decreases.

For Pt_2V, the bent C_{2v} open triangle (*3a*) is found to be the GM, with a Pt–V–Pt angle of 139.3°. Pt–Pt bonding is not observed for the GM doublet states. This is similar to the Pt_2Ti cluster, where, Pt–Pt bonding is also not observed for the GM singlet state. Differences between the singly doped PtTi and PtV clusters are observed for the four and five atom clusters.

The doublet bent C_s Y-shape cluster (*4a*) is found to be the GM for Pt_3V, compared with the C_{2v} kite structure GM of Pt_3Ti. The doublet bent C_s top-capped rhombus structure (*5a*) is found to be the GM for Pt_4V, compared with the W-shaped structure for Pt_4Ti. These differences suggest that Pt-Pt bonding is less favourable for PtV clusters than PtTi clusters, although it appears to be more favourable than for the doubly doped PtTi clusters. A similar C_s twisted pentagonal structure (*6a*) is found to be the GM for both Pt_5V (doublet) and Pt_5Ti (triplet).

As with the singly doped PtTi clusters, it is found that GM planar and "bent-planar" structures are found for the singly doped PtV clusters for 3–6 atoms. When comparing the average Pt–Pt bond lengths, few trends are apparent, with variation being structure dependant. However, more evident trends are observed for Pt–V bonding, where the Pt–V bond length generally increases with increasing spin.

The Bader charge analysis reveals that once again, there is significant charge transfer from the V, becoming positive, to the Pt, becoming negative. As the spin is increased, generally the charge transfer decreases as for PtTi clusters, though there is generally less charge transfer than in PtTi.

4.4.2. Doubly doped

The lowest lying structures for doubly doped PtV clusters are listed in Table 7, corresponding to the structures in Fig. 5. In contrast to the singly doped clusters, GM structures for the doubly doped clusters are all triplets. This is similar to the dimers, where

Table 7
Relative energies (E_{rel}), average bond lengths and average Bader charges for the doubly doped PtV clusters (shown in Fig. 5), for varying multiplicities (2S + 1).

2S + 1	Cluster	E_{rel} (eV)	Pt–Pt (Å)	Pt–V (Å)	V–V (Å)	Ave. Pt Charge |e|	Ave. V Charge |e|
Pt_1V_2							
1	3a	0.00	–	2.41	1.80	−0.68	0.21
3	3a	−0.03	–	2.43	1.79	−0.74	0.33
5	3a	0.60	–	2.45	1.76	−0.77	0.30
7	3b	1.74	–	2.15	2.46	−0.71	0.27
7	3a	1.77	–	2.45	1.97	−0.71	0.46
9	3b	1.00	–	2.15	2.49	−0.83	0.60
Pt_2V_2							
1	4a	0.00	–	2.38	1.95	−0.74	0.77
3	4a	−0.21	–	2.41	1.91	−0.75	0.62
5	4a	0.34	–	2.40	2.19	−0.83	0.86
7	4a	0.34	–	2.39	2.70	−0.81	0.86
9	4b	1.33	2.77	2.44	2.80	−0.70	0.62
Pt_3V_2							
1	5a	0.00	–	2.39	2.01	−0.67	0.99
3	5a	−0.31	–	2.40	2.02	−0.69	1.14
5	5a	0.15	–	2.39	2.47	−0.70	1.06
7	5b	0.49	2.70	2.44	2.53	−0.66	0.76
9	5c	1.51	2.70	2.47	3.06	−0.59	0.89
9	5d	1.56	2.62	2.45	2.68	−0.54	0.83
Pt_4V_2							
1	6a	0.00	2.86	2.33	2.33	−0.55	1.15
3	6b	−0.08	–	2.34	2.58	−0.56	1.19
5	6c	0.33	2.60	2.37	2.61	−0.53	0.96
7	6d	0.62	2.58	2.44	2.52	−0.51	1.07
9	6e	1.35	2.63	2.44	2.72	−0.51	1.10

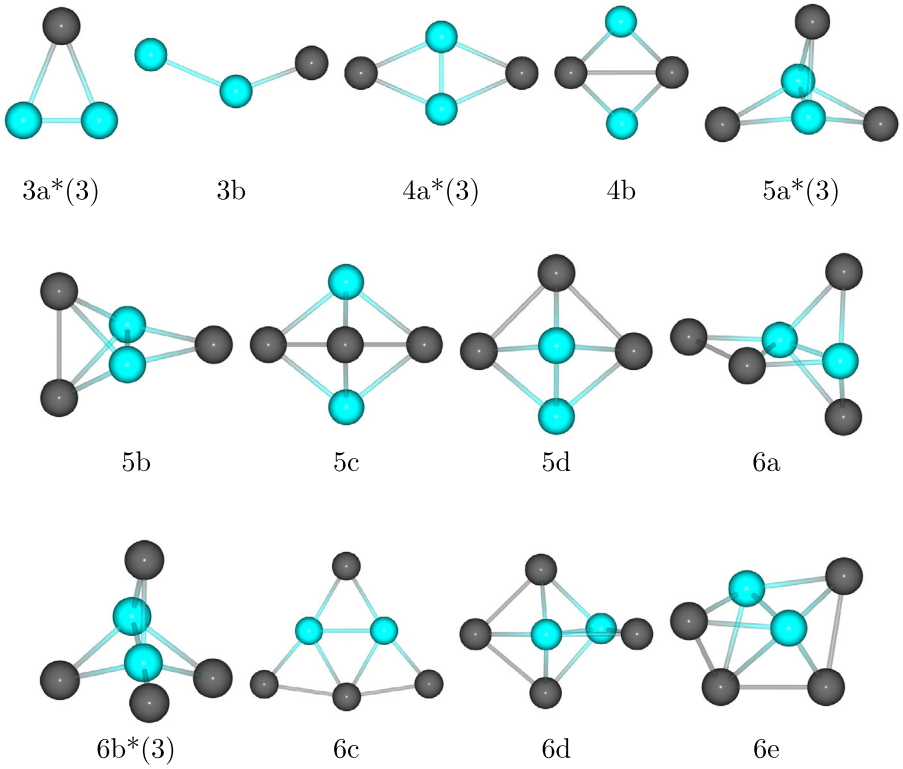

Fig. 5. Low energy structures found for $Pt_{x-2}V_2$ clusters, from Pt_1V_2 to Pt_4V_2, with varying spin multiplicities. GM clusters for all sizes are specified (*). Numbers in brackets show at which spin multiplicity the GM is found.

the triplet and quartet states (for V_2 and PtV respectively) are found to be most energetically favourable. Furthermore, energetic penalties associated with higher spin states are reduced compared to the singly doped clusters.

The GM structures for the doubly doped PtV clusters are similar to those for doubly doped PtTi clusters. The 3-atom closed C_{2v} triangle (*3a*), with a Ti–Pt–Ti angle of 43.3°, 4-atom bent C_{2v} rhombus (*4a*), 5-atom D_{3h} (*5a*) and 6-atom C_{3v} (*6b*) structures are identified

as GM for $Pt_{x-2}V_2$ clusters. As mentioned previously, cluster growth leads to maximisation of V–V and Pt–V bonding and minimisation of Pt-Pt bonding. Once again, due to the low number of Pt–Pt bonds, it is hard to draw trends from the average Pt–Pt bond lengths. Average Pt–V and V–V bond lengths show that generally, as the spin increases, so do the bond lengths. As for PtTi, the doubly doped PtV clusters exhibit a distinct 2D/3D transition. This occurs between the 4-atom bent C_{2v} rhombus and 5-atom D_{3h} structures.

Once again, there is generally reduced charge transfer for the PtV clusters, compared with the PtTi clusters. Furthermore, for the doubly doped PtV clusters, there is greater overall charge transfer to the Pt and a reduction in the positive charges on the V atoms, compared to the singly doped PtV clusters. A general reduction in the amount of charge transfer is also seen as the spin is increased, as with the other systems. However, PtV_2 is anomalous, as an increase in charge transfer is seen as the spin is increased. It can also be seen that, generally as the cluster size increases, the average Pt negative charge decreases (as there are a greater number of Pt atoms), whilst the average positive charge on the V atoms increases.

5. Conclusions

From the results presented in this study, it is apparent that, whilst spin has a significant effect on pure Pt clusters, varying effects are found for the doped PtTi and PtV clusters. Favourable energies are observed up to the septet state for pure Pt clusters. GM structures are found to be planar or "bent-planar" for Pt cluster sizes 3–6. However, partial spin quenching is observed when Pt clusters are doped with Ti or V.

Increasing the spin of PtTi clusters generally results in higher energies. The triplet state is favourable for Pt_5Ti and $PtTi_2$, however GM structures are found for the singlet state for all other PtTi clusters studied. For the singly doped clusters, again planar and "bent-planar" structures are located as the GM for the 3–6 atom clusters. For the doubly doped PtTi clusters, initially more planar structures are favoured, however GM 5–6 atom structures adopt 3D conformations.

The GM structures for 3–6 atom singly doped PtV clusters are all doublets. However, the doubly doped clusters, all have triplet GM. As with the PtTi clusters, planar and "bent-planar" structures are found for the 3–6 atom singly doped PtV clusters, although different GM structures are found for the 4–5 atom clusters. Similar GM structures are found for the PtV and PtTi clusters, exhibiting the same 2D/3D transition between the 4- and 5-atom clusters.

Acknowledgements

This research was funded through RCUK doctoral training centre in hydrogen, fuel cells and their applications (EP/G037116/1). The authors thank COST Action MP0903: "Nanoalloys as Advanced Materials: From Structure to Properties and Applications". The computations described in this paper were performed using The University of Birmingham's BlueBEAR HPC service, which was purchased through HEFCE SRIF-3 funds and via our membership of the UK's HPC Materials Chemistry Consortium, which is funded by EPSRC (EP/F067496), this work made use of the facilities of HECToR, the UK's national high-performance computing service, which is provided by UoE HPCx Ltd at the University of Edinburgh, Cray Inc and NAG Ltd, and funded by the Office of Science and Technology through EPSRC's High End Computing Programme.

Appendix A. Supplementary data

Supplementary data associated with this article can be found, in the online version, at http://dx.doi.org/10.1016/j.comptc.2013.06.033.

References

[1] R.L. Johnston, Atomic & Molecular Clusters, Taylor & Francis, London, 2002.
[2] S. Vajda, M.J. Pellin, J.P. Greeley, C.L. Marshall, L.A. Curtiss, G.A. Ballentine, J.W. Elam, S. Catillon-Mucherie, P.C. Redfern, F. Mehmood, P. Zapol, Subnanometre platinum clusters as highly active and selective catalysts for the oxidative dehydrogenation of propane, Nature Materials 8 (2009) 213–216.
[3] R. Ferrando, J. Jellinek, R.L. Johnston, Nanoalloys: from theory to applications of alloy clusters and nanoparticles, Chemical Reviews 108 (2008) 845–910.
[4] Nanoalloys: from Theory to application, Faraday Discussions 138 (2008) 440.
[5] A. Chandan, M. Hattenberger, A. El-kharouf, S. Du, A. Dhir, V. Self, B.G. Pollet, A. Ingram, W. Bujalski, High temperature (HT) polymer electrolyte membrane fuel cells (PEMFC) a review, Journal of Power Sources 231 (2013) 264–278.
[6] P. Mani, R. Srivastava, P. Strasser, Dealloyed binary PtM3 (M = Cu, Co, Ni) and ternary PtNi3M (M = Cu, Co, Fe, Cr) electrocatalysts for the oxygen reduction reaction: Performance in polymer electrolyte membrane fuel cells, Journal of Power Sources 196 (2011) 666–673.
[7] J.A. Keith, G. Jerkiewicz, T. Jacob, Theoretical investigations of the oxygen reduction reaction on Pt(111), Chemphyschem: A European Journal of Chemical Physics and Physical Chemistry 11 (2010) 2779–2794.
[8] P.C. Jennings, B.G. Pollet, R.L. Johnston, Theoretical studies of Pt–Ti nanoparticles for potential use as PEMFC electrocatalysts, Physical Chemistry Chemical Physics: PCCP 14 (2012) 3134–3139.
[9] P.C. Jennings, B.G. Pollet, R.L. Johnston, Electronic properties of PtTi nanoalloys and the effect on reactivity for use in PEMFCs, The Journal of Physical Chemistry C 116 (2012) 15241–15250.
[10] E. Antolini, R.R. Passos, E.A. Ticianelli, Electrocatalysis of oxygen reduction on a carbon supported platinum vanadium alloy in polymer electrolyte fuel cells, Electrochimica Acta 48 (2002) 263–270.
[11] B. Wang, Recent development of non-platinum catalysts for oxygen reduction reaction, Journal of Power Sources 152 (2005) 1–15.
[12] R. Koffi, C. Coutanceau, E. Garnier, J.-M. Léger, C. Lamy, Synthesis, characterization and electrocatalytic behaviour of non-alloyed PtCr methanol tolerant nanoelectrocatalysts for the oxygen reduction reaction (ORR), Electrochimica Acta 50 (2005) 4117–4127.
[13] C.W. Bezerra, L. Zhang, H. Liu, K. Lee, A.L. Marques, E.P. Marques, H. Wang, J. Zhang, A review of heat-treatment effects on activity and stability of PEM fuel cell catalysts for oxygen reduction reaction, Journal of Power Sources 173 (2007) 891–908.
[14] P. Boski, S. Dennler, J. Hafner, Strong spin-orbit effects in small Pt clusters: geometric structure, magnetic isomers and anisotropy, The Journal of Chemical Physics 134 (2011) 034107.
[15] V. Kumar, Y. Kawazoe, Evolution of atomic and electronic structure of Pt clusters: Planar, layered, pyramidal, cage, cubic, and octahedral growth, Physical Review B 77 (2008) 205418.
[16] H. Yuan, H. Chen, A. Kuang, B. Wu, Spinorbit effect and magnetic anisotropy in Pt clusters, Journal of Magnetism and Magnetic Materials 331 (2013) 7–16.
[17] C. Heredia, V. Ferraresi-Curotto, M. López, Characterization of Ptn ($n = 212$) clusters through global reactivity descriptors and vibrational spectroscopy, a theoretical study, Computational Materials Science 53 (2012) 18–24.
[18] A. Sebetci, Does spin-orbit coupling effect favor planar structures for small platinum clusters?, Physical Chemistry Chemical Physics: PCCP 11 (2009) 921–925
[19] K. Bhattacharyya, C. Majumder, Growth pattern and bonding trends in Ptn ($n = 213$) clusters: Theoretical investigation based on first principle calculations, Chemical Physics Letters 446 (2007) 374–379.
[20] L.-S. Wang, H. Wu, H. Cheng, Photoelectron spectroscopy of small chromium clusters: observation of even-odd alternations and theoretical interpretation, Physical Review B 55 (1997) 12884–12887.
[21] J. Zhao, Q. Qiu, B. Wang, J. Wang, G. Wang, Geometric and electronic properties of titanium clusters studied by ultrasoft pseudopotential, Solid State Communications 118 (2001) 157–161.
[22] R. Gupta, Lattice relaxation at a metal surface, Physical Review B 23 (1981) 6265–6270.
[23] A.P. Sutton, J. Chen, Long-range FinnisSinclair potentials, Philosophical Magazine Letters 61 (1990) 139–146.
[24] J.N. Murrell, R.E. Mottram, Potential energy functions for atomic solids, Molecular Physics 69 (1990) 571–585.
[25] R.L. Johnston, Evolving better nanoparticles: genetic algorithms for optimising cluster geometries, Dalton Transactions (2003) 4193.
[26] S. Heiles, A.J. Logsdail, R. Schäfer, R.L. Johnston, Dopant-induced 2D-3D transition in small Au-containing clusters: DFT-global optimisation of 8-atom Au–Ag nanoalloys., Nanoscale 4 (2012) 1109–1115.
[27] P.A. Derosa, J.M. Seminario, P.B. Balbuena, Properties of small bimetallic NiCu clusters, The Journal of Physical Chemistry A 105 (2001) 7917–7925.
[28] C.J. Heard, R.L. Johnston, A density functional global optimisation study of neutral 8-atom Cu–Ag and Cu–Au clusters, The European Physical Journal D 67 (2013) 34.
[29] S. Heiles, R.L. Johnston, Global optimization of clusters using electronic structure methods, International Journal of Quantum Chemistry (2013).
[30] A.J. Logsdail, Z.Y. Li, R.L. Johnston, Development and optimization of a novel genetic algorithm for identifying nanoclusters from scanning transmission electron microscopy images, Journal of Computational Chemistry 33 (2012) 391–400.

[31] P. Giannozzi, S. Baroni, N. Bonini, M. Calandra, R. Car, C. Cavazzoni, D. Ceresoli, G.L. Chiarotti, M. Cococcioni, I. Dabo, A. Dal Corso, S. de Gironcoli, S. Fabris, G. Fratesi, R. Gebauer, U. Gerstmann, C. Gougoussis, A. Kokalj, M. Lazzeri, L. Martin-Samos, N. Marzari, F. Mauri, R. Mazzarello, S. Paolini, A. Pasquarello, L. Paulatto, C. Sbraccia, S. Scandolo, G. Sclauzero, A.P. Seitsonen, A. Smogunov, P. Umari, R.M. Wentzcovitch, QUANTUM ESPRESSO: a modular and open-source software project for quantum simulations of materials, Journal of Physics. Condensed Matter: An Institute of Physics Journal 21 (2009) 395502.

[32] M. Valiev, E. Bylaska, N. Govind, K. Kowalski, T. Straatsma, H. Van Dam, D. Wang, J. Nieplocha, E. Apra, T. Windus, W. de Jong, NWChem: a comprehensive and scalable open-source solution for large scale molecular simulations, Computer Physics Communications 181 (2010) 1477–1489.

[33] M.B. Airola, M.D. Morse, Rotationally resolved spectroscopy of Pt[sub 2], The Journal of Chemical Physics 116 (2002) 1313.

[34] H. Grönbeck, W. Andreoni, Gold and platinum microclusters and their anions: comparison of structural and electronic properties, Chemical Physics 262 (2000) 1–14.

[35] S. Yanagisawa, T. Tsuneda, K. Hirao, An investigation of density functionals: the first-row transition metal dimer calculations, The Journal of Chemical Physics 112 (2000) 545.

[36] M. Doverstal, B. Lindgren, U. Sassenberg, C.A. Arrington, M.D. Morse, The 3Π0u X3Δ1g band system of jet-cooled Ti2, The Journal of Chemical Physics 97 (1992) 7087.

[37] E.M. Spain, M.D. Morse, Bond strengths of transition-metal dimers: titanium-vanadium(TiV), vanadium dimer, titanium-cobalt (TiCo), and vanadium-nickel (VNi), The Journal of Physical Chemistry 96 (1992) 2479–2486.